Thin Solid Films 519 (2011) 2907–2913

Contents lists available at ScienceDirect

Thin Solid Films

journal homepage: www.elsevier.com/locate/tsf

Optical properties of soda-lime float glass from spectroscopic ellipsometry

Ron A. Synowicki *, Blaine D. Johs, Andrew C. Martin

J.A. Woollam Co., Inc., 645 M. Street, Suite 102, Lincoln, NE 68508, USA

ARTICLE INFO

Keywords:
Spectroscopic ellipsometry
Float glass
Soda-lime glass
Refractive index
Birefringence
Air side
Tin side
Index gradient

ABSTRACT

Optical properties of soda-lime glass manufactured by the float process were investigated using spectroscopic ellipsometry and intensity transmission measurements. Thickness and optical properties of surface layers on the air and tin sides were determined with ellipsometry. The tin side surface layer shows a graded refractive index with a non-linear profile. Intensity transmission data were used to quantify absorption in the bulk glass. Transmission-mode generalized ellipsometry characterized residual birefringence in the bulk glass. Birefringence effects on ellipsometric delta data were corrected using a simple empirical offset with 1/wavelength dependence. A general optical model for soda-lime glass is presented which can be used for subsequent analysis of coated soda-lime glass and other transparent substrates.

1. Introduction

Soda-lime glass, commonly known as “float glass” is used in everyday products and devices such as solar cells, household mirrors, automobile glass, architectural building windows, etc. Float glass is manufactured in large flat sheets by pouring molten glass onto a flowing bath of liquid tin. The molten glass “floats” on top of the liquid tin for several minutes while it cools from an initial temperature of near 1100 °C to approximately 600 °C before being removed from the tin bath. During this floating stage some tin diffuses into the lower surface of the glass [1–9], and this “tin” side of the glass subsequently exhibits significantly different optical properties than the opposite “air” side.

Understanding the bulk optical properties of soda-lime float glass and the surface layers which form on the air and tin sides is important for subsequent characterization of deposited coatings on soda-lime glass. This is particularly important for applications such as thin-film solar cells, where coatings are typically deposited onto the air side, but often characterized by measurements made through the tin side and the glass substrate. In order for such measurements through the glass substrate to be accurate it is desirable to characterize the tin side surface layer and effects such as absorption and birefringence in the bulk glass [10]. Birefringence in float glass may be residual from the manufacturing process, or can be induced after manufacture as strain birefringence via the heat tempering process [1].

Float glass typically has a characteristic green tint, resulting in absorption over a broad spectral range from visible to infrared wavelengths. This bulk absorption and green tint are generally attributed to addition of iron oxide into the glass [6]; other additives can also be used to produce different colors of soda-lime glass.

In this work we use spectroscopic ellipsometry [11–14], generalized ellipsometry [12–16], and intensity transmission data to characterize the surface and bulk optical properties of soda-lime float glass. The ellipsometric psi data for uncoated glass are generally sensitive to the refractive index, while ellipsometric delta data are extremely sensitive to the thickness and optical properties of the surface layers. Ellipsometric data acquired from both surfaces are used to identify and characterize the air and tin sides. Intensity transmission data are more sensitive to bulk optical properties and added to the analysis to characterize bulk absorption in the glass.

Refractive index birefringence [10] in the bulk glass was investigated using transmission-mode ellipsometric data acquired through the samples at normal incidence. It was found that tempered soda-lime glass shows significant stress birefringence effects on ellipsometric data when acquired through the glass substrate. These birefringence effects also affect ellipsometric data acquired in reflection-mode through the glass substrate at higher, oblique angles of incidence; so an empirical correction term with 1/wavelength dependence was introduced in the analysis to correct for bulk birefringence effects on reflection-mode data.

2. Experiment

2.1. Samples measured

Three samples of transparent soda-lime “clear” float glass were investigated using spectroscopic ellipsometry and intensity transmission data. The samples studied were 1.6 mm, 3.3 mm, and 5.6 mm

* Corresponding author. Tel.: +1 402 477 7501; fax: +1 402 477 8214.
E-mail address: rsynowicki@jawoollam.com (R.A. Synowicki).

0040-6090/$ – see front matter © 2010 Elsevier B.V. All rights reserved.
doi:10.1016/j.tsf.2010.12.110

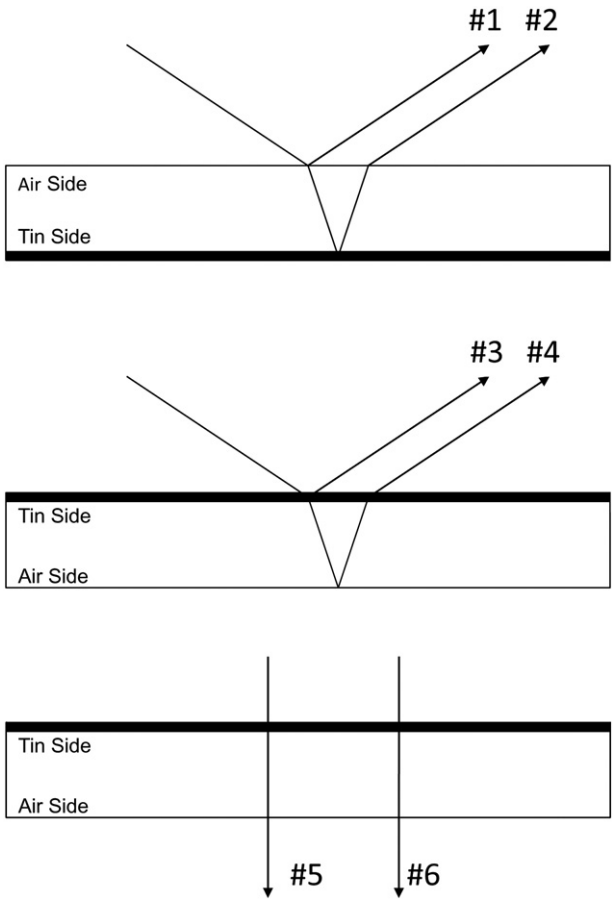

Fig. 1. Six data scans acquired on float glass samples. Reflection-mode ellipsometry data were acquired from the upper surface (data types #1 and #3) and through the substrate (data types #2 and #4) from the air and tin sides. Intensity transmission (data type #5) and transmission-mode generalized ellipsometry measurements (data type #6) through the glass samples were also performed.

thick (as measured with a caliper). The 3.3 mm sample was heat tempered, while the others were untreated. Each sample exhibited a visual green tint easily observed by looking through the edge of the glass.

2.2. Data acquisition

Data were acquired using a J.A. Woollam Company VASE® spectroscopic ellipsometer and analyzed using J.A. Woollam Company CompleteEASE® software. This software allows for simultaneous analysis of reflection and transmission-mode ellipsometric data from multiple directions, as well as intensity transmission and reflectance data. The software also enables birefringence calculation and correction factors for birefringence effects.

Several data types were acquired from each sample as shown in Fig. 1. First, reflection-mode ellipsometric data were acquired from the air and tin surfaces of the glass (data types #1 and #3). These ellipsometric data were acquired at multiple angles of incidence between 55° and 80° over the spectral range from 300 nm to 2500 nm. Measurements were also performed through the front side (first surface) of each sample while ellipsometric data from the back surface (second surface) were acquired (data types #2 and #4).

Since the glass samples are transparent and reflective on both sides it is important to account for unwanted reflections from the back surface for data types #1 and #3, and unwanted reflections from the front surface when measuring through the substrate for data types #2 and #4. In thicker samples, reflections from the front and back surfaces are spatially separated and do not overlap, but in thinner samples the two beams can overlap at the detector. For data types #1 and #3 reflections from the back surface were suppressed by using translucent index matching tape applied to the back side of the samples [17]. For data types #2 and #4, the beam was focused to a smaller spot to avoid unwanted reflections from the upper surface when measuring the back surface through the substrate.

To investigate absorption in the bulk glass, measurements of transmitted intensity were performed at normal incidence through each glass sample using the VASE® instrument (data type #5). The resulting intensity transmission data were analyzed to determine the extinction coefficient, k(λ) of the bulk glass versus wavelength.

Refractive index birefringence in the bulk glass was investigated using transmission-mode ellipsometric data (data type #6). These "Generalized ellipsometry" scans used multiple incident polarization states acquired through each sample at normal incidence over the spectral range from 300 nm to 2500 nm. A generalized ellipsometry scan records polarization conversion between the p- and s-components of the beam caused by birefringence in the bulk glass [14–16]. These cross-polarization terms are then analyzed to quantify phase retardance between the p- and s-polarized components due to very small amounts of refractive index anisotropy in the bulk glass.

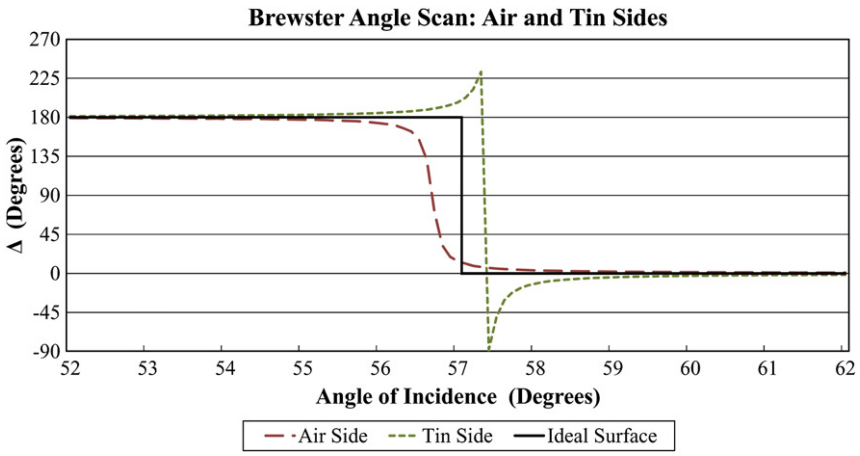

Fig. 2. Difference between air and tin surfaces of float glass compared to an ideal smooth surface. Scans were made through the Brewster angle at λ = 500 nm using angle steps of 0.1°. The angle of incidence where delta=90 degrees identifies Brewster's angle. The upward and downward slopes in delta through Brewster's angle indicate surface layers with higher and lower refractive index than the bulk glass for the air and tin sides, respectively. This method can be used to identify the air and tin sides of soda-lime float glass.

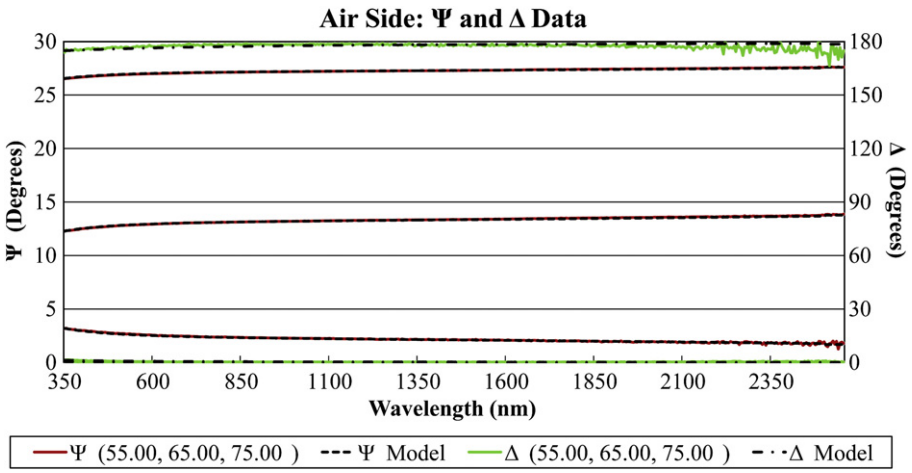

Fig. 3. Experimental ellipsometric data and model fits to air side of 1.6 mm clear float glass. Fitting psi data gives the refractive index. To fit the delta data a surface layer with lower refractive index than the bulk was added.

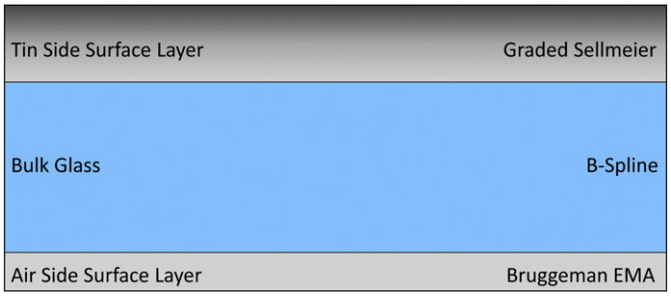

Fig. 4. Analysis model for soda-lime glass showing the different layers and refractive index models used for each. The air side surface layer was modeled using an EMA mixture of air and bulk glass. The tin side was modeled using a Sellmeier function with graded refractive index. The bulk glass was modeled using a B-Spline function for the optical constants n & k.

If significant birefringence is present in the bulk glass, it is important to correct for these birefringence effects when reflection-mode ellipsometric data are acquired through the glass substrate at oblique angles from the second or back surface (data types #2 and #4). This was done on the tempered glass sample by acquiring ellipsometric data through the sample from both the air and tin sides at 70° angle of incidence. This angle was chosen because it is often used for ellipsometric analysis of coatings on float glass. An empirical correction factor (delta offset) with 1/wavelength dependence was added to the analysis to account for the bulk birefringence effects on the ellipsometric delta data.

3. Results and discussion

3.1. Surface effects

3.1.1. Identification of air and tin sides

The first step in our analysis is to identify the air and tin sides of float glass. Two methods are presented here. The first method compares the refractive indices from the air and tin sides of the glass. The air side of soda-lime glass typically shows a refractive index of approximately 1.51 to 1.52 at visible wavelengths. The tin side of float glass generally shows a refractive index that is approximately 0.02 to 0.03 higher than that of the air side [2–9]. The side with higher refractive index identifies the tin side.

The second technique involves measuring the behavior of surface layers on both sides of the glass, and requires no data analysis. Differences are easily observed in the ellipsometric delta data when scanning through the Brewster angle [16] as shown in Fig. 2. Using a single wavelength of 500 nm in the transparent

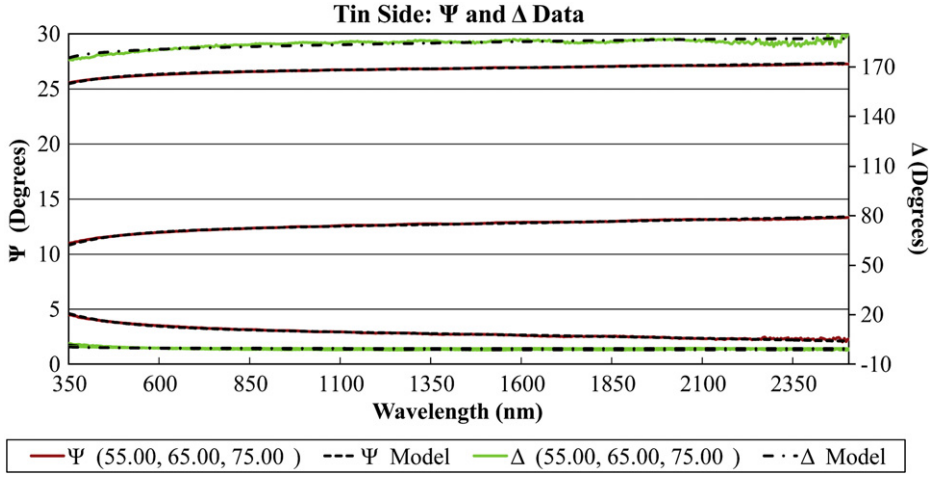

Fig. 5. Experimental ellipsometric data and model fits to the tin side of 1.6 mm clear float glass. A surface layer with higher refractive index than the bulk was added to the tin side.

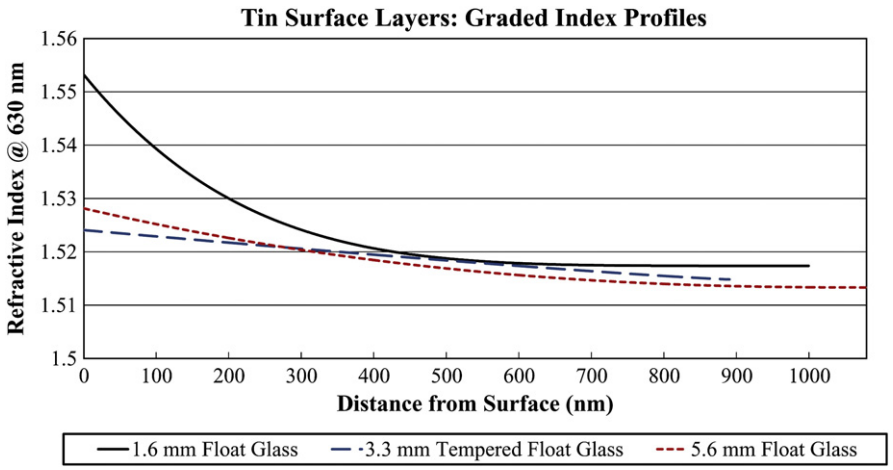

Fig. 6. Tin side refractive index profiles versus depth for three float glass samples. The index gradients are attributed to diffusion of tin into the glass. Results are shown at 630 nm wavelength.

spectral range and scanning with small angle steps of 0.1° through the Brewster angle allows easy identification of the air and tin sides. The choice of 500 nm in our experiment was arbitrary; any wavelength in the transparent spectral range should work.

Fig. 2 shows scans of the air and tin sides (data types #1 and #3) through the Brewster angle compared to an ideally smooth surface, which would produce a step function. The position of the Brewster angle (where delta = 90°) indicates that the air side surface has a lower refractive index than the tin side, which shows a higher Brewster angle. Also note the upward curvature in delta when approaching Brewster's angle for the tin side, and the downward trend for the air side, indicating surface layers with higher and lower indices than the bulk glass, respectively. We consider this Brewster angle method advantageous because it requires no data analysis: the position and shape behavior of the experimental delta data through the Brewster angle alone identifies the air and tin sides.

3.1.2. Analysis of air side

The bulk glass refractive index can be modeled effectively using Cauchy, Sellmeier, Basis Spline (B-Spline) or other refractive index dispersion function [11–13,18]. A surface layer with an index lower than that of the bulk glass is modeled using a Bruggeman Effective Medium Approximation (EMA) [19], which models the air side surface layer as a fixed percentage mixture of 50% glass and 50% void. As the index of the bulk glass is varied the surface layer index varies in response using this model, but maintains a fixed 50% void fraction, so the air side surface layer always has a lower refractive index that the bulk glass. The thickness of this surface layer was fit along with the refractive index of the bulk glass to data type #1, with fit results shown in Fig. 3.

3.1.3. Analysis of tin side

Analysis of the tin side surface layer is more challenging because this surface contains a significant amount of diffused tin. A graded diffusion profile has been confirmed by a variety of experimental techniques [2–9], and suggests that the tin side surface layer should have a gradient in its optical properties as well.

Analysis of the tin side surface layer starts with the analysis of air side described above. It is possible to fix the bulk glass index and air side surface layer determined above and fit for the properties of the tin side. However, since the analysis software allows simultaneous analysis of data acquired from both sides of the glass the method used here fits properties of both surface layers and the bulk glass index. Data acquired from the tin surface (data type #3) were added to the analysis, and a surface layer with higher index than the bulk glass was added to the tin side. The model constructed is shown in Fig. 4. A Sellmeier dispersion

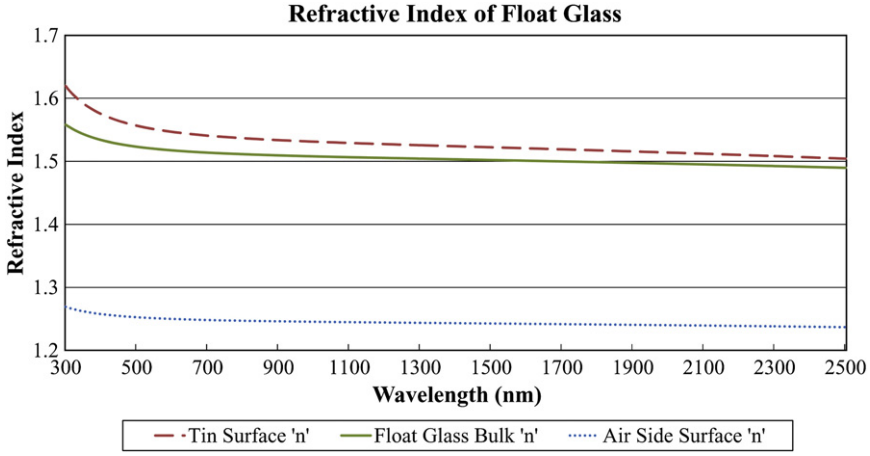

Fig. 7. Refractive indices of surface layers and bulk 1.6 mm clear soda-lime glass. Note the tin side and air side surface layers show index values higher and lower than the bulk glass, respectively.

Table 1
Thickness of air and tin side surface layers for three soda-lime float glass samples.

Samples	Graded tin thickness	Air side surface layer
1.6 mm clear float glass	982.8 nm	1.5 nm
3.3 mm tempered float glass	877.7 nm	3.7 nm
5.6 mm clear float glass	1064.8 nm	1.8 nm

Table 2
Goodness-of-fit parameter (Mean Squared Error) for analysis of tin side surface layer for 3 float glass samples. Best results with lowest MSE were obtained when fitting a graded refractive index with non-linear profile.

Samples	Single layer MSE	Linear grading MSE	Non-linear grading MSE
1.6 mm clear float glass	4.60	2.81	1.28
3.3 mm tempered float glass	2.49	1.53	1.53
5.6 mm clear float glass	4.10	2.91	1.17

function was used to describe the refractive index of the tin surface layer [13]. The thickness and refractive index of the tin side surface layer were fit along with the refractive index of the bulk glass and the thickness of the air side layer. The tin side surface layer was then allowed to have a graded or varying index profile with depth. Both linear and non-linear grading profiles were investigated. Significant improvement was observed when fitting the grading magnitude, and additional improvement was seen when fitting the grading profile shape. Results are shown in Figs. 5–7 and Tables 1 and 2.

Note the Sellmeier model chosen for the tin side surface layer assumes the surface layer is non-absorbing and optically isotropic (no birefringence). In reality this thin surface layer may exhibit small amounts of absorption and birefringence similar to the bulk glass; however, in the very small path length provided by the surface layer these effects are assumed small enough to not be noticed. Thus absorption and birefringence effects are considered in this work to be properties of the bulk glass rather than surface effects. However, the magnitude and profile of the index gradient on the tin surface were significant enough to improve the analysis.

3.2. Bulk properties

3.2.1. Bulk absorption in soda-lime glass

Soda-lime float glass shows significant absorption at visible and infrared wavelengths, including a visible green tint. Since this absorption is a property of the bulk glass, rather than a surface effect it can be quantified by analyzing intensity transmission data acquired through the sample (data type #5). Using the thickness of each glass sample as measured with a caliper, and fixing the model results derived in Section 3.1.3 above (see also Fig. 4), the intensity transmission data were analyzed to extract the extinction coefficient k(λ) as a function of wavelength for each sample. Fig. 8 shows intensity transmission data and model fit results for the 1.6 mm thick sample. Note that the decreased transmission in the range 500 nm to 1500 nm is a distinctive identifying characteristic of soda-lime glass. This bulk absorption must be accounted for when analyzing transmission data acquired through coated soda-lime glass samples. In such coated samples bulk absorption in the glass substrate must be separated from absorption in deposited coatings. Fig. 9 shows the bulk refractive index and extinction coefficient versus wavelength for the 1.6 mm float glass sample. Note the intensity transmission measurement is sensitive to very small k-values on the order of 10^{-5} or less due to the long 1.6 mm path length through the glass.

3.2.2. Birefringence effects in bulk glass at normal incidence

It is possible to investigate low level birefringence in the bulk glass using transmission-mode ellipsometry where the long path length through the sample gains sensitivity to refractive index anisotropy.

Transmission-mode ellipsometric data were acquired through each sample at normal incidence to test for birefringence effects in the bulk glass (data type #6). A generalized ellipsometry scan using multiple incident polarization states was used. Results are shown in Fig. 10. Note that the tempered glass shows significant retardance between the p- and s-polarization components. This is attributed to stress birefringence on the order of 10^{-6} or lower for the samples studied here induced by the heat tempering and fast quenching process [1]. These bulk birefringence properties affect the measured ellipsometric delta data, and must be corrected for when fitting ellipsometric data acquired through the substrate (data types #2 and #4 discussed below).

3.2.3. Correcting for bulk birefringence effects at oblique angles of incidence

Reflection-mode ellipsometry measurements are typically performed at oblique angles of incidence. For measurements acquired through the bulk glass (data types #2 and #4), birefringence effects are observed in ellipsometric delta data, but not psi. It is possible to correct for these birefringence effects on the measured delta data using a simple offset with 1/wavelength dependence in the analysis

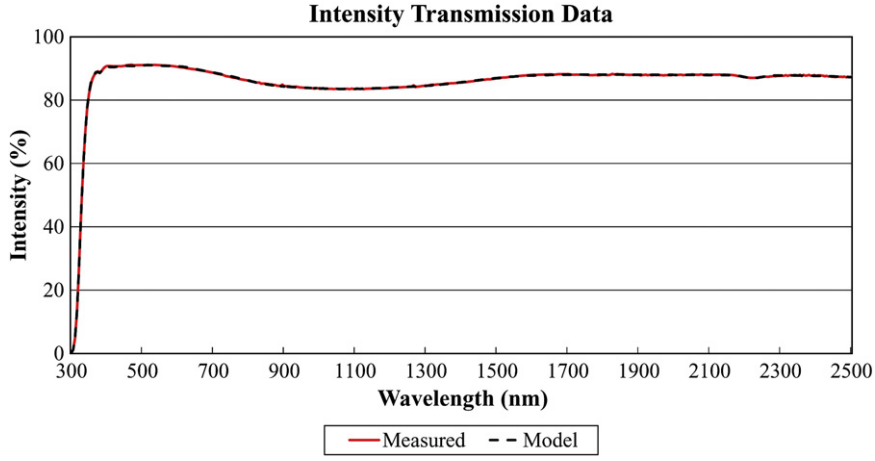

Fig. 8. Intensity transmission data and model fits to 1.6 mm clear float glass to determine the extinction coefficient k(λ) of the bulk glass. The pronounced decrease in transmission between 500 nm and 1500 nm is characteristic of soda-lime glass.

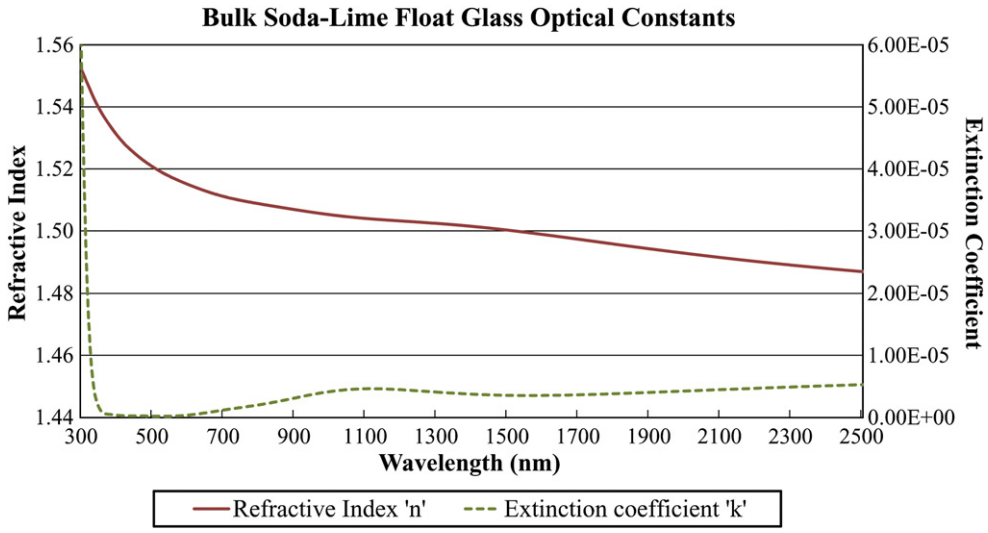

Fig. 9. Bulk optical constants n & k of 1.6 mm clear float glass. Ellipsometric data gives the refractive index n, while intensity transmission data were analyzed to extract the very small extinction coefficient k-values.

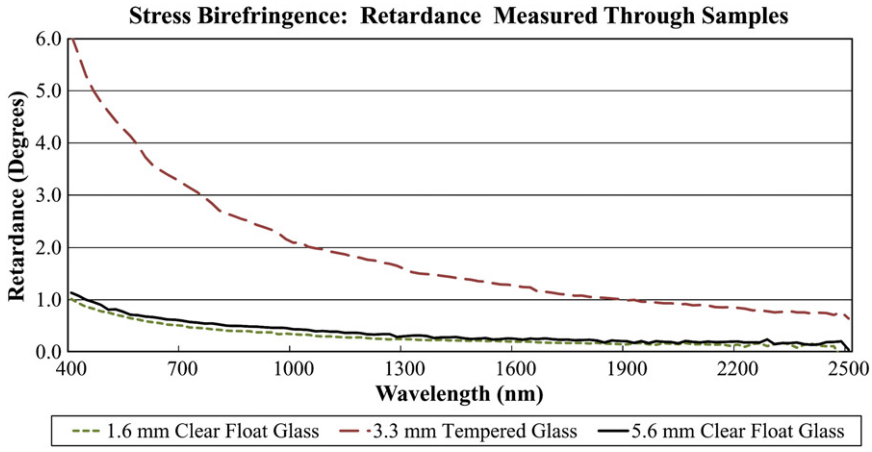

Fig. 10. Retardance induced by birefringence in soda-lime glass determined by transmission-mode generalized ellipsometry measurements through the sample at normal incidence. The tempered glass shows significant stress birefringence effects. The refractive index birefringence was estimated to be 10^{-6} or lower.

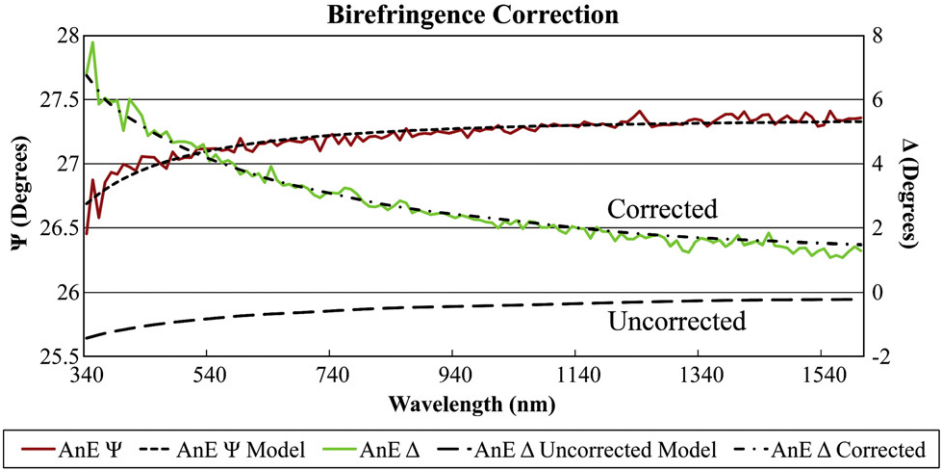

Fig. 11. Ellipsometric delta data acquired through the 3.3 mm tempered glass substrate. Birefringence in the bulk glass affects the measured delta data, and is corrected by fitting an empirical delta offset term with $1/\lambda$ dependence. Both uncorrected and corrected model fits are shown.

model. Fig. 11 shows uncorrected and corrected model fits to psi-delta data acquired through the tempered glass substrate. When measuring through the substrate at oblique angles, such correction enables subsequent analysis of films coated on the opposite side.

4. Conclusion

A general model for optical analysis of soda-lime float glass has been developed. The model allows optical characterization of the bulk glass properties and surface layers on the air and tin sides of float glass. Further, the model allowed us to quantify absorption and birefringence effects in the bulk glass and correct for these effects. The techniques developed here on soda-lime float glass should be applicable to colored or tinted soda-lime glass, as well as other types of glass. This work should be useful for subsequent analysis of films coated onto soda-lime glass and other transparent substrates.

References

[1] W.F. Smith, Principles of Materials Science and Engineering, 2nd Edition McGraw-Hill Publishers, Inc., New York, 1990.
[2] L. Colombin, A. Jelli, J. Riga, J.J. Pireaux, J. Verbist, J. Non-Cryst. Solids 24 (1977) 253.
[3] L. Colombin, H. Charlier, A. Jelli, G. Debras, J. Verbist, J. Non-Cryst. Solids 38/39 (1980) 551.
[4] W.E. Baitinger, P.W. French, E.L. Swarts, J. Non-Cryst. Solids 38/39 (1980) 749.
[5] B. Dugnoille, O. Virlet, Appl. Opt. 33 (1994) 5853.
[6] F. Lamouroux, N. Can, P.D. Townsend, B.W. Farmery, D.E. Hole, J. Non-Cryst. Solids 212 (1997) 232.
[7] P.D. Townsend, N. Can, P.J. Chandler, B.W. Farmery, R. Lopez-Heredero, A. Peto, L. Salvin, D. Underdown, B. Yang, J. Non-Cryst. Solids 223 (1998) 73.
[8] Y. Hayashi, K. Matsumoto, M. Kudo, J. Non-Cryst. Solids 282 (2001) 188.
[9] M.K. Tiwari, M.H. Modi, G.S. Lodha, A.K. Sinha, K.J.S. Sawhney, R.V. Nandedkar, J. Non-Cryst. Solids 351 (2005) 2341.
[10] E. Hecht, Optics, 4th Edition Addison-Wesley Publishing, San Francisco, 2002.
[11] H.G. Tompkins, W.A. McGahan, Spectroscopic Ellipsometry and Reflectometry, John Wiley & Sons, Inc., New York, 1999.
[12] H.G. Tompkins, E.A. Irene, Handbook of Ellipsometry, William Andrew Publishing, 2005.
[13] H. Fujiwara, Spectroscopic Ellipsometry, John Wiley & Sons, Inc., Chichester, 2007.
[14] R.M.A. Azzam, N.M. Bashara, Ellipsometry and Polarized Light, Elsevier Publishing, Amsterdam, 1977.
[15] M. Schubert, Thin Solid Films 313–314 (1998) 323.
[16] B. Johs, J.A. Woollam, C.M. Herzinger, J. Hilfiker, R. Synowicki, C.L. Bungay, SPIE CR 72 (1999) 30.
[17] R.A. Synowicki, Phys. Status Solidi C 5 (2008) 1085.
[18] B. Johs, Phys. Status Solidi (a) 205 (2008) 715.
[19] D.E. Aspnes, J.B. Theeten, F. Hottier, Phys. Rev. B 20 (1979) 3292.